JOURNAL OF SOLID STATE CHEMISTRY 87, 222–228 (1990)

Equation of State of $MnAs_{0.88}P_{0.12}$

HELMER FJELLVÅG AND SVEIN STØLEN

Department of Chemistry, University of Oslo, N-0315 Oslo 3, Norway

AND WALTER A. GROSSHANS AND THOMAS KRÜGER

Fachberich Physik, Universität—GH—Paderborn, D-4790 Paderborn, Federal Republic of Germany

Received December 18, 1989

The influence of external pressure, up to 30 GPa, on the structural properties of $MnAs_{0.88}P_{0.12}$ has been studied for temperatures between 300 and 450 K by energy dispersive X-ray diffraction using synchrotron radiation. $MnAs_{0.88}P_{0.12}$ undergoes a very large, continuous volume contraction when subjected to pressure. The experimental pV relationship is discussed on the basis of the first-order Birch and Murnaghan equations of state, and the structural changes are discussed in relation to similar observations for isostructural (MnP-type) phases. The experimental results at 300, 350, and 450 K are in excellent agreement with earlier estimations of the temperature dependence of the compressibility which were based on the chemical pressure concept with starting point in the equivalency of the p, T phase diagram of MnAs and the x, T phase diagram of $MnAs_{1-x}P_x$. The isothermal bulk modulus B_0 and its pressure derivative B_0' are, according to the Murnaghan equation of state, respectively 18 GPa and 10 at 300 and 450 K and respectively 10 GPa and 18 at 350 K. Values for the Gibbs energy and the entropy as 300 K are tabulated as functions of applied pressure.

Introduction

The structural and magnetic properties of several MnP- and NiAs-type phases depend strongly on temperature and applied pressure. There are different sources of pressure; it can be applied externally (e.g., under hydrostatic conditions) or produced internally through chemical substitution. The different types of pressure may for certain systems have very similar effects on structural properties and phase boundaries in the corresponding phase diagrams. One such example is given by MnAs, of which the p, T phase diagram (*1*) for applied external pressures below 1 GPa closely resembles the complex x, T phase diagram of the pseudobinary $MnAs_{1-x}P_x$ system, $x < 0.20$ (*2*).

An anomalous heat capacity effect is observed for $MnAs_{1-x}P_x$ with origin in a magnetic low to high spin conversion. The effect was explained phenomenologically by assuming a strong coupling between the conversion and the degree of orthorhombic distortion of the MnP-type structure (*3*, *4*). The large and broad heat capacity peak was accounted for by considering the extraordinary strong temperature dependence of the thermal expansion and the compressibility, which in turn yields an anomalous dilational contribution to the heat capacity. No experimental values for the isothermal compress-

0022-4596/90 $3.00

ibility were, however, at hand, and the $\kappa(T)$ relationship was estimated (*3, 4*) based on the similarities of the p, T phase diagram of MnAs and the x, T phase diagram of $MnAs_{1-x}P_x$, using the chemical pressure concept. The objective of the present work is to document experimental values for the isothermal compressibility at some fixed temperatures in order to test the validity of the earlier assumptions on the behaviour of $\kappa(T)$.

The present study focuses on $MnAs_{0.88}P_{0.12}$ which undergoes the low to high spin conversion in the temperature interval between the Néel temperature T_N = 234 K and the transition temperature for the MnP $\rightleftharpoons$ NiAs-type transition, T_D = 460 K. The variation in the unit cell volume was measured by means of X-ray diffraction for applied pressures up to 30 GPa. The obtained data are discussed in relation to a low–high spin conversion model. The structural data obtained are further compared with similar results reported earlier on isostructural phases like CoAs (*5*), FeAs (*5*), CrAs (*6*), MnAs (*7, 8*), FeS (*9*), MnSb (*10*), and MnTe (*10, 11*). The experimentally observed pV relationship is discussed on the basis of the first-order Murnaghan (*12*) and Birch (*13, 14*) equations of state.

Experimental

The $MnAs_{0.88}P_{0.12}$ sample was prepared and characterized as described in Ref. (*2*). The energy-dispersive powder X-ray diffraction study for applied pressures up to 30 GPa was carried out at HASYLAB, Hamburg, using a gasketed diamond anvil cell (*15*). The very intense white synchrotron radiation was collimated before and after hitting the sample, and the scattered intensities were registered by a solid-state X-ray detector system (*15*) providing accurate energy analysis of the diffracted X-rays. The applied pressure was determined by measuring the ruby R1 fluorescence and using a calibration constant of 365 pm/GPa (*16*). The small splinters of ruby were inserted together with the sample into the small cavity in the center of the metal gaskets between the flat faces of the diamond anvil (*17*), thus permitting simultaneous recording of diffraction patterns and fluorescence spectra. In the present experiments, nitrogen was used as a pressure-transmitting medium (*18*) in the study conducted at 300 K (to better assure hydrostatic conditions), whereas no such medium was used in the measurements at 350 and 450 K.

Results

The diffraction patterns collected at 300, 350, and 450 K for applied pressures up to 30 GPa were all consistent with an MnP-type crystal structure with As and P atoms randomly distributed over the nonmetal site. Based on the individual patterns, the pressure dependence of the unit cell dimensions (*a, b, c, V,* space group *Pnma*) were obtained. The results at 300 and 450 K are presented in Fig. 1. The obtained variation at 350 K shows a slightly larger spread. No hysteresis with respect to increasing or decreasing pressure was observed. The rather uniform variation in the unit cell dimensions with pressure at respectively 300 and 450 K clearly indicates that the lack of pressure-transmitting medium does not cause nonhydrostatic conditions large enough to influence these dimensions. However, on changing the pressure, significant variations in the intensities of the individual reflections were frequently observed, which indicates that preferred orientation/texture effects are present.

The pressure dependence of the reduced unit cell volume $V(p)/V_0$ at 300, 350, and 450 K is shown in Fig. 2. The dashed and solid curves represent the variation found

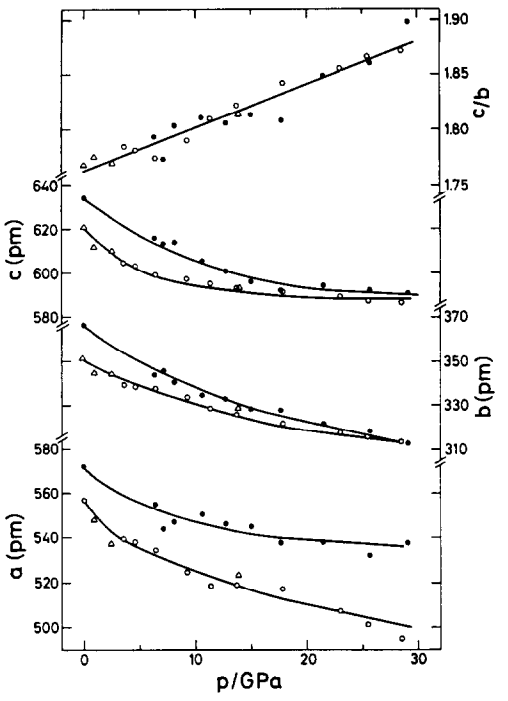

FIG. 1. Pressure dependence of the unit cell dimensions of $MnAs_{0.88}P_{0.12}$ at 300 K (open symbols) and 450 K (solid symbols). Circles and triangles denote results derived upon increasing and decreasing pressure conditions, respectively.

when fitting the observations according to, respectively, the first-order Murnaghan and Birch equations of state. The Birch equation of state anticipates that the isothermal bulk modulus, $B(T, p) = -V(\partial p/\partial V)_T$, varies linearly with pressure, $B = B_0 + B_0'p$, whereas in the other case, a fixed relation for B_0' is assumed. The data analysis was performed according to the analytical expressions; Murnaghan: $p = (B_0/B_0')[(V_0/V)\ B_0' - 1]$; Birch: $p = \frac{3}{2}B_0[(V_0/V)^{7/3} - (V_0/V)^{5/3}][1 + \frac{3}{4}(B_0' - 4)((V_0/V)^{2/3} - 1)]$. The values deduced for B_0 in the present study are roughly independent of the choice of equation, whereas large differencies are found for the pressure derivative B_0', especially for the 350 K data.

The quality of the fit between observed and calculated $V(p)/V_0$ is shown in Fig. 2. The larger value for B_0' at 350 K (Table I) implies a stronger curvature and a smaller compressibility at higher pressures than at 300 and 450 K. This is also reflected in the relative unit cell volumes when compared at e.g., 25 GPa; at 350 K, $V(25\ \text{GPa})/V_0 = 0.79$ whereas at 300 and 450 K, $V(25\ \text{GPa})/V_0 = 0.76$ (for both ratios, calculated uncertainty ± 0.006).

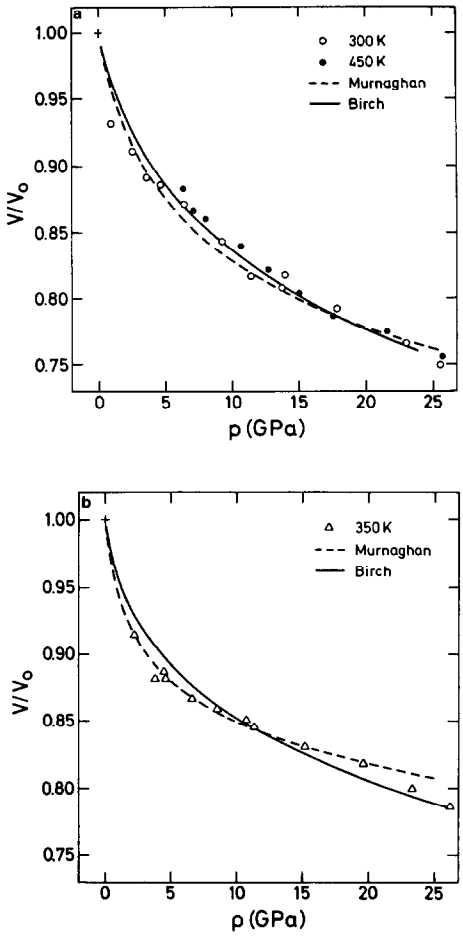

FIG. 2. Reduced unit cell volume as a function of external pressure at (a) 300 and 450 K and (b) 350 K. Dashed and solid curves represent fits based on the Murnaghan and Birch equations of state, respectively.

TABLE I

ISOTHERMAL BULK MODULUS B_0 AND ITS PRESSURE DERIVATIVE B_0' FOR $MnAs_{0.88}P_{0.12}$

	Murnaghan		Birch	
T (K)	B_0 (GPa)	B_0'	B_0 (GPa)	B_0'
300	18	10	20	14
350	10	18	8	60
450	18	10	20	14

Discussion

Structural Properties

All axes, a, b, and c, contract significantly upon increasing pressure. However, the compression is largest along the b-axis. This implies that the c/b ratio, which under certain circumstances can be used as a measure of the degree of the orthorhombic MnP-type distortion, increases with pressure. At high pressures, the ratios become larger than those generally found among the MnP-type arsenides and approach that of, e.g., MnP (*19*). This is in accordance with the findings for FeAs and CoAs (*5*). The behavior of CrAs is different (*6*) by having a negative value for the compressibility along the b-axis, which, however, may be caused by variation in the magnetostrictive forces since the magnetic ordering temperature at ambient pressure is close to room temperature. The observation of increased c/b ratio is further in full accordance with the changes introduced by substituting P for As in, e.g., MnAs (*20*), CrAs (*21*), and $Mn_{1-t}Cr_tAs$ (*22*).

At high temperatures, $T > 460$ K, $MnAs_{0.88}P_{0.12}$ takes the hexagonal NiAs-type structure. During the orthorhombic transition the metal atoms are mainly displaced perpendicularly to the hexagonal axis while the nonmetal atoms are displaced mainly along that axis (*2*). The effect of pressure is to displace the metal and nonmetal atoms in a similar way. According to Lyman and Prewitt (*5*), an interesting aspect of the compression of CoAs is that the longest As–As distance, through which the shortest metal–metal edge-sharing interaction occurs, is not able to contract as much as the other interatomic separations. When this edge is unable to contract anymore, a more anisotropic structure will probably be favored, but only slight indications for a structural phase transition were observed at 7 GPa for CoAs (*5*).

The presently obtained compressibilities are larger than those reported for most other MnP- and NiAs-type phases (see Table II). The compressible phases are characterized by having rather high B_0', which implies that they all become much less compressible upon increasing pressure.

On the Chemical Pressure Concept

In the arsenic-rich samples of $MnAs_{1-x}P_x$ a low to high spin transition takes place between the Néel temperature T_N and the distortion temperature T_D. In a recent heat capacity study of $MnAs_{0.88}P_{0.12}$ a large, broad peak due to this conversion with maximum 30 J K^{-1} mol^{-1} at 347 K was observed (*13, 14*). In order to account for this anomaly, the dilational contribution to the heat capacity was calculated, $C_d = TV\alpha^2\kappa^{-1}$. The temperature dependence of the unit cell volume, and thus also the expansivity, was obtained from high-temperature powder diffraction data. The critical step was hence the estimation of the temperature dependence of the isothermal compressibility. The observed excess heat capacity is shown in Fig. 3; the calculated curve is also included.

The qualitative correspondence between chemical and external pressure is evident in that application of both types reduces the unit cell volume. However, problems with nonrandom distribution or cluster formation of/around the substituting atoms, anisotropic contraction, and nonhydrostatic pressure make a quantitative approach difficult.

TABLE II

ISOTHERMAL BULK MODULUS B_0 AND ITS PRESSURE DERIVATIVE B_0' FOR SOME NiAs- AND MnP-TYPE PHASES AT 293 K

Phase	Structure	EOS	B_0 (GPa)	B_0'	Ref.
CoAs	MnP	Birch	122.7	8.8	(5)
FeAs	MnP	Birch	118.4	7.2	(5)
FeS	NiAs	Birch	34.8	5	(9)
MnAs	MnP	Birch	24	40	(8)
MnSb	MnP	Birch	46	8	(10)
$MnAs_{0.8}Sb_{0.2}$	NiAs	Birch	73	3	(8)
	MnP	Birch	106	8	(8)
MnTe	NiAs	Birch	49.7	5.6	(10)
	MnP	Birch	58.4	3.0	(11)
$MnAs_{0.88}P_{0.12}$	MnP	Murnaghan	18	10	This study
	MnP	Birch	20	14	This study

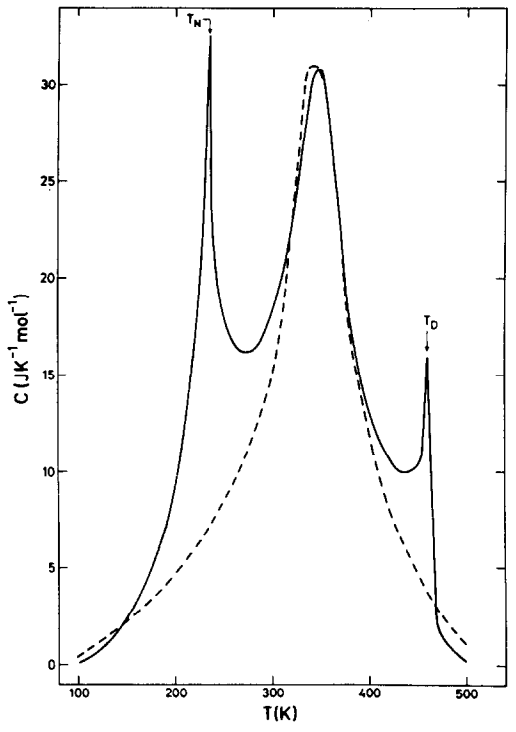

FIG. 3. Excess heat capacity (solid line). Dashed curve, calculated dilational contribution.

Nevertheless, the phase diagram for MnAs under pressure exhibits a striking similarity to the phase diagram for $MnAs_{1-x}P_x$. In the operative chemical pressure concept at low substitution levels (*23*), the chemical pressure is assumed to be proportional to the degree of substitution, $\varepsilon = \Delta p/\Delta x$, and for $MnAs_{0.88}P_{0.12}$ ε is 53 kbar (see below). By using this concept, the compressibility can be calculated since $\kappa = [V^{-1}(\partial V/\partial x)_T/(\partial p/\partial x)_T]$, where $(\partial V/\partial x)_T$ is evaluated from diffraction data. The values obtained for the compressibility in the present study at 300, 350, and 450 K should now be compared with those derived from these model calculations.

The model values obtained for κ at 300, 350, and 450 K were 9, 16, and 9 $\times$ 10^{-11} Pa^{-1}, respectively (*4*). The present experimental values for the bulk modulus are 18, 10, and 18 GPa, respectively, or κ = 5.5, 10, and 5.5 $\times$ 10^{-11} Pa^{-1}. The relation between the experimental and model values for $\kappa(T)$ is seen to be constant, and the compressibility at 350 K is about 80% larger than the corresponding values at 300 and 450 K. However, the experimental numerical values are about 50% lower than those obtained

by the model calculations. A smaller value of κ implies a larger value of ε. As discussed in (*4*) there are several ways of estimating ε on the basis of common phase lines in the p, T and x, T phase diagrams, yielding ε values ranging between 53 and 143 kbar. A smaller value for κ would, however, imply that the calculated dilational heat capacity contribution becomes larger, hence giving a less good fit to the experimentally observed anomaly in the heat capacity. On the other hand, the overall agreement between the estimated and observed compressibilities is surprisingly good when the simplifying assumptions implicit in the chemical pressure concept, e.g., that ε is a constant independent of composition and temperature, that the chemical pressure is anisotropic (nonhydrostatic) in character in the noncubic MnP type phases, etc., are considered. Finally, it should be mentioned that the present experimental study may be the source of the discrepancy toward the parameters derived by means of the chemical pressure concept, since the major part of the experimental data were collected at rather high applied external pressures, resulting in large uncertainties for B_0 due to strong correlation between B_0 and B_0' in the fits.

Thermodynamic Properties

The thermodynamic properties of $MnAs_{0.88}P_{0.12}$ under pressure are evaluated on the basis of the Maxwell relationship

$$(\partial S/\partial p)_T = -(\partial v/\partial T)_p$$

and $\alpha = V^{-1}(\partial V/\partial T)_p$ and $(\partial S/\partial p)_T = -\alpha V$. Then $\Delta S = -\int \alpha V dp$, $\Delta H = \int (V - TV\alpha)dp$, and $\Delta G = \int V dp$, where $\alpha = \alpha(T, p)$ is a function of temperature and pressure. The Gibbs energy change follows directly from the present data. In order to calculate the entropy and enthalpy, the pressure dependence of the expansivity must be known, and this requires a model for the Gibbs energy for the phase under consideration. Using a somewhat complex Gibbs energy function, Guillermet *et al.* (*24*) expressed the expansivity in terms of the compressibility and expansivity at ambient pressure and $d\kappa(T, 0)/dT$ as

$$\alpha(T, p) = \alpha(T, 0) - [d\kappa(T, 0)/dT][p/(1 + B_0' p\kappa(T, 0))],$$

and thus

$$\Delta S = -\int \alpha(T, 0) V dp + d\kappa(T, 0)/dT \int [pV/(1 + B_0' p\kappa(T, 0))]dp.$$

Data evaluated for the Gibbs energy and estimated entropy at 300 K are given in Table III for selected pressures up to 25 GPa. The enthalpy is implicit in Table III. [$(d\kappa(T, 0)/dT$ is estimated from the earlier calculated compressibility curve, having a value of 5×10^{-12} Pa^{-1} K^{-1}.]

TABLE III

THERMODYNAMIC PROPERTIES OF $MnAs_{0.88}P_{0.12}$

P (GPa)	$\Delta_0^p S_m^0(p)$ (J K^{-1} mol^{-1})	$\Delta_0^p G_m^0(p)$ (k J mol^{-1})
0.0001	72.5	9.63
0.25	80.0	14.1
0.50	93.2	18.6
0.75	106.5	23.0
1.00	119.8	27.4
2.00	179.0	44.7
3.00	232.5	61.7
4.00	286.2	78.4
5.00	340.1	94.9
10.0	611.0	175.
15.0	884.2	251.
20.0	1153.5	325.
25.0	1434.7	396.

Acknowledgments

This work has been founded in part by the German Minister for Research and Technology (BMFT) under Contract 05 340 AX BO and has received financial support from the Norwegian Research Council for Science and the Humanities.

References

1. N. MENYUK, J. A. KAFALAS, K. DWIGHT, AND J. B. GOODENOUGH, *Phys. Rev.* **177**, 942 (1969).

2. H. FJELLVÅG, A. KJEKSHUS, AND S. STØLEN, *J. Solid State Chem.* **64,** 123 (1986).
3. H. FJELLVÅG, F. GRØNVOLD, A. KJEKSHUS, AND S. STØLEN, *J. Phys. C* **20,** 3005 (1987).
4. A. K. LABBAN, E. F. WESTRUM JR., H. FJELLVÅG, F. GRØNVOLD, A. KJEKSHUS, AND S. STØLEN, *J. Solid State Chem.* **70,** 185 (1987).
5. P. S. LYMAN AND C. T. PREWITT, *Acta Crystallogr. B* **40,** 14 (1984).
6. V. I. KAMENEV AND E. A. ZAVADSKII, *Sov. Phys. Solid. State Engl. Transl.* **20,** 541 (1978).
7. N. P. GRAZHDANKINA AND A. M. BURKHANOV, *Sov. Phys. JETP Engl. Transl.* **23,** 1013 (1966).
8. H. FJELLVÅG, H. D. HOCHHEIMER, AND W. HÖNLE, *Phys. Lett. A* **118,** 293 (1986).
9. H. E. KING JR. AND C. T. PREWITT, *Acta Crystallogr. B* **38,** 1877 (1982).
10. H. NAGASAKI, I. WAKABAYASHI, AND S. MINOMURA, *J. Phys. Chem. Solids* **30,** 329 (1969).
11. M. MIMASAKA, I. SAKAMOYO, K. MURATA, Y. FUJII, AND A. ONODERA, *J. Phys. C* **20,** 4689 (1987).
12. F. D. MURNAGHAN, *Proc. Natl. Acad. Sci.* **30,** 244 (1944).
13. F. BIRCH, *J. Geophys. Res.* **57,** 227 (1952).
14. F. BIRCH, *J. Appl. Phys.* **9,** 279 (1938).
15. W. A. GROSSHANS, E. F. DUESING, AND W. B. HOLZAPFEL, *High Temp.-High Pressures* **16,** 539 (1984).
16. G. J. PIERMARINI, S. BLOCK, J. D. BARNETT, AND R. A. FORMAN, *J. Appl. Phys.* **46,** 2774 (1975).
17. W. B. HOLZAPFEL, *in* "High Pressure Chemistry" (H. Kelm, Ed.), p. 177, Reidel, Amsterdam (1978).
18. R. LESARE, S. A. EKBERG, L. H. JONES, R. L. MILLS, L. A. SCHWALBE, AND D. SHIFERL, *Solid State Commun.* **32,** 131 (1971).
19. A. ROGER AND R. FRUCHART, *Mater. Res. Bull.* **3,** 253 (1968).
20. H. FJELLVÅG, A. F. ANDRESEN, AND K. BÄRNER, *J. Magn. Magn. Mater.* **46,** 29 (1984).
21. K. SELTE, H. HJERSING, A. KJEKSHUS, A. F. ANDRESEN, AND P. FISCHER, *Acta Chem. Scand. A* **29,** 695 (1975).
22. A. F. ANDRESEN, K. BÄRNER, H. FJELLVÅG, A. KJEKSHUS, H. RAGER, U. SONDERMANN, AND S. STØLEN, *J. Magn. Magn. Mater*, submitted.
23. A. ZIĘBA, R. ZACH, H. FJELLVÅG, AND A. KJEKSHUS, *J. Phys. Chem. Solids* **48,** 79 (1987).
24. A. F. GUILLERMET, P. GUSTAVSON, AND M. HILLERT, *J. Phys. Chem. Solids* **46,** 1427 (1985).